International Journal of Biological Macromolecules 199 (2022) 150–161

Contents lists available at ScienceDirect

International Journal of Biological Macromolecules

journal homepage: www.elsevier.com/locate/ijbiomac

Folate functionalized chitosan nanoparticles as targeted delivery systems for improved anticancer efficiency of cytarabine in MCF-7 human breast cancer cell lines

Deepa Geethakumari [a], Anoop Bhaskaran Sathyabhama [a], Krishnapriya Raji Sathyan [a], Dhaneesha Mohandas [a], Jisha V. Somasekharan [b], Sajeevan Thavarool Puthiyedathu [a,*]

[a] National Centre for Aquatic Animal Health, Cochin University of Science and Technology, Fine Arts Avenue, Kochi 682 016, Kerala, India
[b] Research and Post Graduate Department of Chemistry, MES Keveeyam College, Valanchery 676552, Kerala, India

ARTICLE INFO

Keywords:
Cytarabine
Chitosan
Folate receptors
MCF-7 cells
A-549 cells

ABSTRACT

Anticancer drug cytarabine, has been widely used for treating haematological malignancies while it has minimal activity against solid tumours, which demands continuous infusion leading to high dose cytarabine toxicity. In this study, folate conjugated chitosan nanoparticles (FCCNP) were used for targeted delivery of cytarabine in breast adenocarcinoma cell lines by making use of the overexpressed folate receptors on the surface of MCF-7. Folate was conjugated to chitosan using carbodiimide. FCCNPs show spherical morphology with a size of<50 nm. Zeta potential of + 45.2 mV and PDI of 0.98 from DLS measurement confirms a stable monodisperse nanoformulation. Cytotoxicity was studied in folate receptor positive, MCF-7 and folate receptor negative, A-549 cell lines. Increased cellular uptake of the drug incorporated nanoparticles was confirmed in MCF-7 cells with fluorophore, squaraine 650 compared to A-549 cells. The relative fold of expression of genes involved in apoptosis such as *bax, cyt c and cas 9* were upregulated. The present in vitro study confirms improved cytotoxicity of cytarabine folate conjugated chitosan nanoparticles in MCF-7 cells.

1. Introduction

Cytarabine (Ara-C, 1-β-D-arabinofuranosyl cytosine), a pyrimidine nucleoside analogue, is a first-line drug for the treatment of myeloid leukaemia, non-Hodgkin's lymphoma and meningeal leukaemia. Cytarabine is phosphorylated by deoxycytidine kinase that leads to the inhibition of DNA polymerase and DNA repair activity and causes S phase arrest, further trigger apoptosis followed by cell death. It has been reported that cytarabine shows little activity against solid tumours, whereas it is found therapeutically effective in combination with other antitumour compounds. However, to show an appreciable effect against solid tumours, the concentration of the drug needs to be increased, which might cause side effects on non-targeted cells and tissues. The half - life of cytarabine in plasma is very short due to the rapid deamination of the pyrimidine ring leads to the formation of inactive 1-β-D-arabinofuranosyl uracil (Ara-U) in the liver and kidney [1]. The enzymatic degradation of the drug can be reduced by encapsulating it into drug delivery systems which enhances bioavailability and reduces frequency of dosing as well as undesirable side effects [2].

Polymeric nanoparticles have been emerging as pharmacological vectors for the targeted drug delivery in cancer therapy. The tumour microenvironment characteristics are exploited to design drug delivery systems for specifically directing anticancer drugs to the tumour milieu. Targeted drug delivery by polymeric nanoparticles aids specific and rapid internalisation of the desired drug into a target cell and minimise the drug induced toxic side effects to normal tissues. Polymeric nanoparticles with diameters ranging from 10 to 1000 nm are promising entities for drug delivery and retention [3], enhancing drug stability, solubility, and controlled release in targeted tumour tissue. Nanoparticle-based delivery relies on size-dependent, passive targeting or active targeting through site-specific ligands [4]. However, passive targeting of nanoparticles through enhanced permeability and retention effect (EPR effect) alone is insufficient to achieve a high level of the drug at the targeted tissue [5]. Active targeting can improve the efficiency of the delivery systems by functionalising the polymer by targeting ligands such as antibodies, folic acid, biotin and peptides. Active targeting diminishes the non-specific action of passive targeting through specific binding of receptors overexpressed on cancer cells. Targeted delivery

* Corresponding author.
E-mail address: sajeev@cusat.ac.in (S. Thavarool Puthiyedathu).

https://doi.org/10.1016/j.ijbiomac.2021.12.070
Received 7 August 2021; Received in revised form 16 November 2021; Accepted 11 December 2021
Available online 30 December 2021

systems increase the therapeutic efficiency of the drug by enhancing pharmacokinetics and biodistribution [6].

Chitosan (poly-β(1 → 4)-2-amino-2-deoxy-D-glucose) is one of the most naturally abundant biopolymers widely used in drug delivery and tissue engineering. Chitosan nanoparticles are promising drug delivery systems due to their biocompatibility, low immunogenicity and biodegradability, and ability to form gels, films, fibres, and particles. Chitosan is reported to show antitumour activity through membrane disrupting and apoptosis inducing activities [7]. Functional groups such as hydroxyl and amino groups on the backbone of chitosan make it an attractive candidate for the conjugation of cancer-targeting ligands such as folate, antibodies, peptides etc. The cationic nature of chitosan improves the targeting due to the affinity towards negatively charged biological membrane. Folic acid is an ideal tumour marker for targeted drug delivery as folate receptors (FR) are overexpressed on the surface of human tumour cells such as the breast, ovary, uterus, kidney, colon and lungs. The expression of folate receptors on tumour cells is around 100–300 times higher when compared to normal cell [8]. Folate conjugated on the nanoparticles bind to folate receptors on tumour cells and get internalised via receptor-mediated endocytosis and enhance the retention of payload in tumour environment [9]. Lack of immunogenicity, low molecular weight, relatively high stability and ease of synthesis make folic acid a useful ligand for tumour targeting compared to antibodies [10]. Several folate conjugated therapeutics enter into clinical trials for cancer therapy. Folate conjugated nanoparticles enter into the tumour through passive as well as active targeting via receptor-mediated endocytosis. It has been reported that the optimal amount of FA moieties that can be used for targeting was 0.1 – 0.2 μmol folate/mg polymer [11].

Recent studies have shown that folate conjugated chitosan nanoparticles enhance the drug retention in tumour mass and site-specific delivery by folate receptor-mediated endocytosis in FR positive cells. It has been reported that the expression of folate receptors is higher in MCF-7 cells compared to normal cells [12]. Ridha et al reported that the anti-cancer effect of doxorubicin and mitoxantrone was enhanced while encapsulating in folate-apoferritin-conjugated cationic solid lipid nanoparticles [13]. Folate conjugated chitosan nanoparticles loaded with ligustrazine showed higher intracellular accumulation in FR positive MCF-7 cell lines than in FR negative A549 cells [14]. Though cytarabine has been widely used for treating haematological malignancies, it has minimal activity against solid tumours due to the short half-life of the drug, which demands continuous infusion leading to high dose cytarabine toxicity. However, the targeted delivery of cancer drugs to tumour sites can reduce the toxic side effects of such medications. Hence this study was carried out to evaluate the potency of folate conjugated chitosan nanoparticles (FCCNP) for targeted delivery of cytarabine in breast adenocarcinoma cell lines by making use of the overexpressed folate receptors on the surface of MCF-7.

2. Materials and methods

2.1. Materials

Chitosan (Medium molecular weight), Sodium Tripolyphosphate (TPP), folic acid, 1-Ethyl-3-(3-dimethylaminopropyl) carbodiimide (EDC), N-hydroxy succinimide (NHS) 3–[4,5–dimethylthiazol–2–yl] –2,5–diphenyltetrazoliumbromide (MTT) and cytarabine were purchased from Sigma – Aldrich (St. Louis, MO, USA). All other reagents used in the study were of analytical grade. Cell lines of human breast adenocarcinoma (MCF-7), human lung adenocarcinoma (A-549) and murine fibroblast (L929) were procured from NCCS, Pune, India and cultured in Dulbecco's Modified Eagle's Medium (DMEM / F-12) supplemented with 10% FBS (Gibco, India).

2.2. Synthesis of folate conjugated chitosan

Folate conjugated chitosan was synthesised according to carbodiimide chemistry. The carboxyl group of folic acid was activated by 1-Ethyl-3-(3-dimethylaminopropyl) carbodiimide (EDC) in the presence of N- hydroxy succinimide (NHS) as reported in previous studies [15]. Equimolar concentrations of folate, EDC and NHS were dissolved in DMSO and stirred for 1 h at room temperature to activate folic acid. Chitosan solution (5 mg/mL) was added to the activated folate and stirred overnight in the dark, followed by the precipitation of the solution by adjusting the pH to 9 using 1 N NaOH. The precipitate obtained was further dialysed against phosphate buffer for 72 h followed by double distilled water for another 72 h and was lyophilised. The lyophilised powder was characterised and used for nanoparticle synthesis.

2.3. Characterisation of folate conjugated chitosan

Conjugation of folate with chitosan was characterised using Fourier Transform Infrared Spectrophotometer (FTIR) and ^{1}H NMR. FTIR spectra of samples were obtained using (Thermo Nicolet, Avatar 370, USA) by dispersing the sample in KBr pellet and scanned in the range of 4000 – 400 cm^{-1}. The ^{1}H NMR spectra was recorded using NMR 400 MHz spectrometer (Bruker Advance III), and chemical shifts were recorded.

2.4. Synthesis of cytarabine loaded folate conjugated chitosan nanoparticles

Ionic gelation method described by Calvo et al was adopted for the synthesis of blank and cytarabine loaded folate conjugated chitosan nanoparticles with slight modifications [16]. Folate conjugated chitosan was dissolved in 1% acetic acid, and the pH was adjusted to 5.5 using 0.1 M NaOH. Cytarabine was added to the FA-CS solution followed by the dropwise addition of TPP solution (0.4% w/v) under magnetic stirring. The suspension was stirred for one hour and centrifuged at 15,000 rpm for 30 min to collect nanoparticles. The obtained precipitate was washed thrice using distilled water to remove the unencapsulated payload. After washing, the precipitate was lyophilised and stored for further experiments.

2.5. Morphology, particle size and zeta potential

Morphology and size of the nanoparticles were observed under High Resolution Transmission Electron Microscope (HR-TEM, JEOL, JEM – 2100). A drop of nanoparticle suspension was placed on a copper grid, gets air dried and observed with TEM. The hydrodynamic diameter and zeta potential of FCCNP were studied by dynamic light scattering (DLS) based on photon correlation spectroscopy (Horiba Scientific, Nanopartica, Nanoparticle analyser SZ – 100, Japan). The samples were dispersed in Milli Q, and the measurement was done at 25 °C with a scattering angle of 90^{0}.

2.6. Entrapment efficiency

The entrapment efficiency of FCCNPs was determined by estimating the concentration of unentrapped cytarabine. The concentration of unentrapped cytarabine was quantified with UV– Visible Spectrophotometer by taking absorbance at 277 nm, and the supernatant of corresponding blank nanoparticles without cytarabine was taken as reference. The entrapment efficiency and drug loading efficiency (%) were calculated as per the following equation (Eq.1 & 2) in which C_C is the initial concentration of cytarabine and C_{FC} is the concentration of unentrapped cytarabine in the supernatant, W_C is the amount of entrapped cytarabine and W is the weight of nanoparticles.

Entrapment efficiency (%) = $C_C - C_{FC}/ C_C$ X 100 (1)

Table 1
qRT -PCR primer sequences used for relative expression of apoptotic genes.

Genes	Primer sequences	*Size (bp)*
bcl-2 [20]	5′-TGGTGGTTTGACCTTTAGAGA-3′ (F) 5′-AGGTCTGATCATTCTGTTC-3′ (R)	217
bax [20]	5′-TGCTTCAGGGTTTCATCCAG-3′ (F) 5′-GGCGGCAATCATCCTCTG-3′ (R)	170
cas 9 [20]	5′-CCTCAAACTCTCAAGAGCAC-3′ (F) 5′-GAGTCAGGCTCTTCCTTTG-3′ (R)	241
cyt c [21]	5′-GGAGGCAAGCATAAGACTGG-3′ (F) 5′-GTCTGCCCTTTCTCCCTTCT-3′ (R)	203
GAPDH [20]	5′-CAAGGAGTAAGACCCCTGGAC-3′ (F) 5′-TCTACATGGCAACTGTGAGGAG-3 (R)	136

Drug Loading (%) = W_C / W X 100 (2)

2.7. In vitro release kinetics

The release of cytarabine from folate conjugated chitosan nanoparticles was studied at pH 6.4 and 7.4, pH equivalent to the tumour microenvironment and blood respectively. FCCNPs with a concentration of 1 mg/1ml were dispersed in phosphate buffer of pH 6.4 and 7.4 and were dialysed (MW cut off – 10,000 Da) in 10 ml of release buffer at 37 °C for 72 h. At regular intervals, 1 ml of the sample was taken and replaced by an equal volume of fresh buffer. The concentration of cytarabine released was calculated by UV spectrophotometry at 277 nm. The experiment was carried out in triplicate, and the percentage of cumulative release was calculated.

2.8. Cytotoxicity studies

The cytotoxicity of FCCNP was studied on both folate receptor positive, human breast adenocarcinoma cell lines (MCF-7) and folate receptor negative, human lung adenocarcinoma cell lines (A-549) using MTT assay [17]. Cells grown in Dulbecco's Modified Eagle's Medium (DMEM) medium with 10% FBS were seeded in 96 well plate with a density of 1 × 10^4 cells per well and incubated with 5% CO_2 at 37 °C. After 24 h the medium was replaced and treated with different concentrations of cytarabine and FCCNP (0.025 – 0.4 μM) for 72 h. After incubation, media were replaced with fresh medium, and 20 μl MTT (5 mg/ ml) was added to each well and kept under dark for 4 h. Then, 200 μl DMSO was added to each well, and the absorbance was read at 570 nm in a microplate reader (TECAN Infinite M 200, Switzerland), and the percentage of relative cell viability was calculated with respect to the control ie, cells without treatment.

2.9. Intracellular uptake of nanoparticles by MCF-7 cells

The cell uptake of FCCNPs was studied using a fluorescent dye, Squaraine 650 (SQ 650) in MCF-7 and A-549 cells [18]. The dye was added along with the drug, cytarabine during ionic gelation process. Cells were seeded in 12 well plates with a density of 2 × 10^5 cells per well. Both cells were incubated with SQ 650 loaded FCCNPs for 2, 4, 6 and 12 h and compared with cells without treatment. Cells were washed with ice-cold PBS thrice after incubation and visualised under fluorescence microscope (Leica, Switzerland). Relative fluorescence intensity was determined using Varioskan Lux multimode microplate reader (Thermo Fischer Scientific, USA)

2.10. Acridine Orange/ ethidium bromide (AO/ EB) dual staining

The morphological changes of apoptosis in the FCCNP treated cells were visualized by acridine orange (AO) and ethidium bromide (EB) dual staining. AO/EB staining was used to differentiate the morphological changes of live and apoptotic cells [19] MCF 7 cells were grown in 24 well plates with a density of 1x10^6 cell per well. The cells were treated with IC_{50} concentration of FCCNP for 72 h. After incubation, the cells were washed with PBS and stained with 10 μl of dual stain containing 100 μg/ml AO and 100 μg/ ml EB and kept for 1 min. After incubation, cells were washed with PBS to remove excess stain and visualised under a fluorescent microscope with an excitation filter at 480 nm.

2.11. Apoptosis assay using Annexin V by flow cytometry

Apoptosis induced by FCCNP was also studied by quantifying the apoptotic cells by flow cytometry using Muse™ Annexin V apoptosis kit. MCF-7 cells were treated with FCCNP of IC_{50} concentration and cytarabine of the same concentration for 72 h. After the incubation, 100 μl of

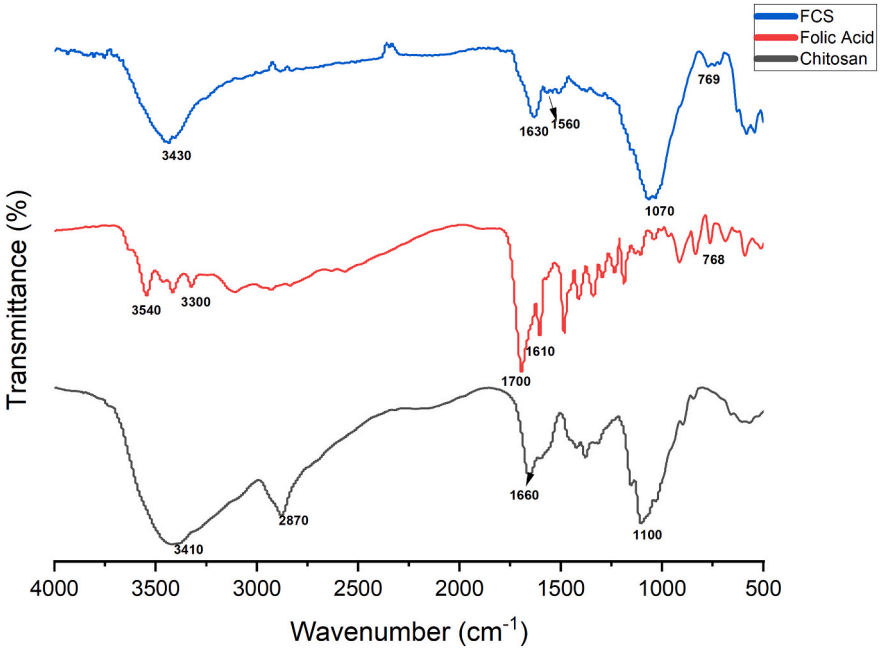

Fig. 1. FTIR spectra of Chitosan, Folic acid and Folate conjugated Chitosan (FCS).

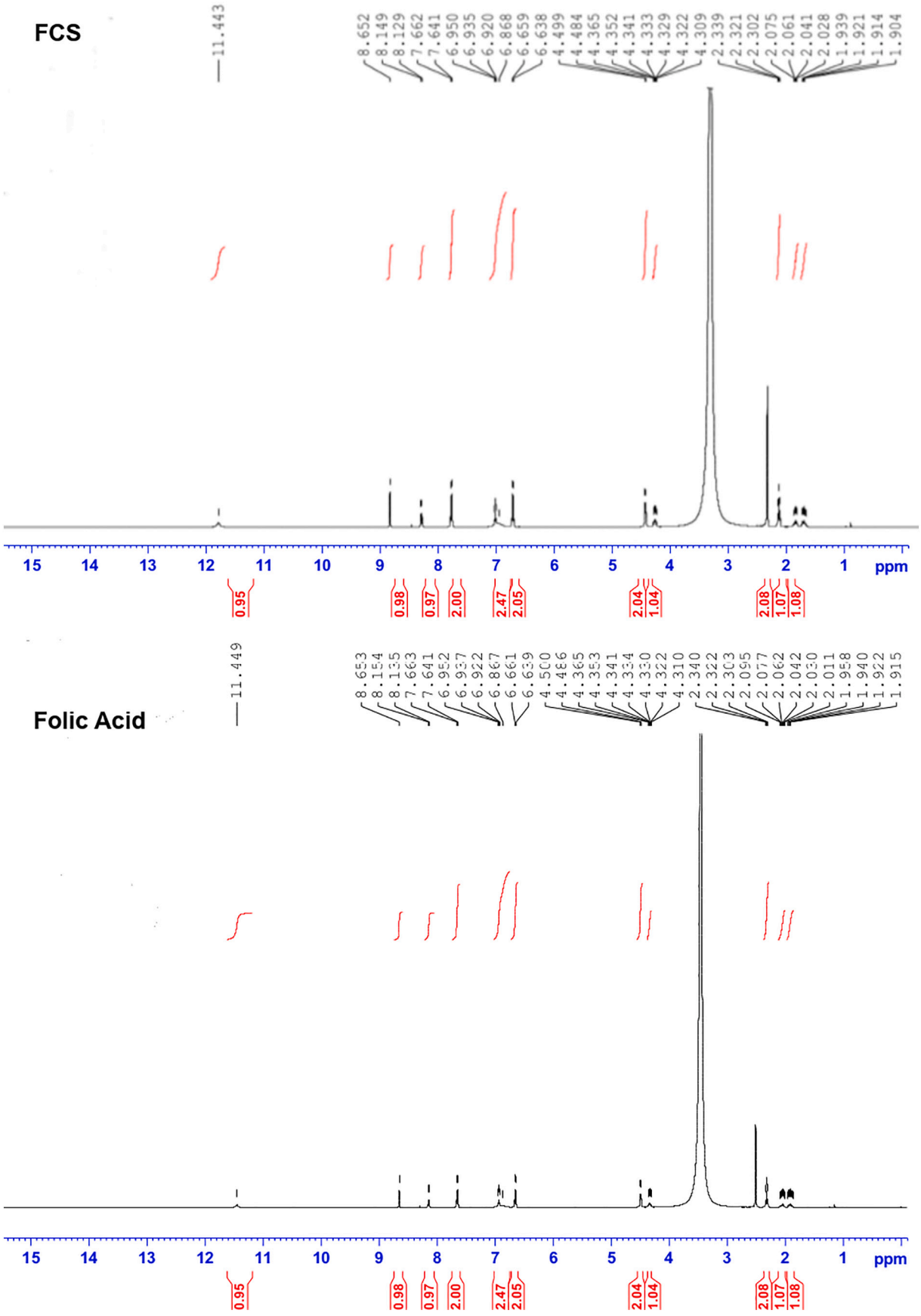

Fig. 2. ^{1}H NMR spectra of Folic Acid (a) Folate conjugated Chitosan (FCS) (b).

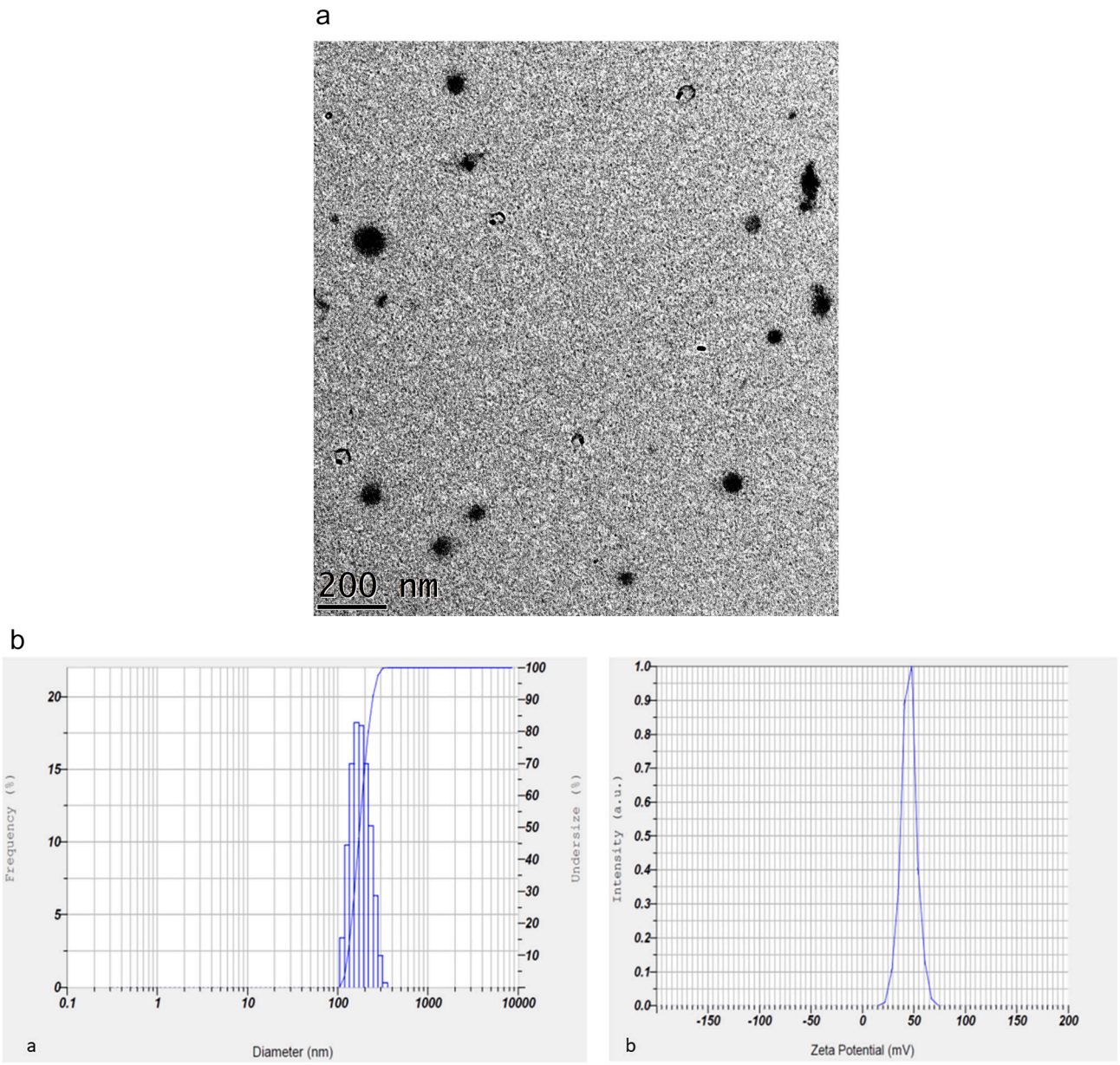

Fig. 3. TEM image showing morphology of FCCNP with particle size of<50 nm. The size distribution (a) and zeta potential (b) of from dynamic light scattering.

cell suspension was taken by trypsinisation and mixed with 100 µl of the the Muse™ Annexin V & Dead Cell Reagent. The tubes were mixed and vortexed at a minimal speed for few seconds and incubated for 20 min at room temperature in the dark. After 20 min, the cells were analysed in a flow cytometer with the aid of Muse flow cytometry software, Muse FCS 3.0 software.

2.12. qRT -PCR analysis for relative expression of apoptotic genes

Quantitative real-time polymerase chain reaction (qRT-PCR) was employed to evaluate the expression of the genes, *bcl-2, bax, cyt c* and *cas9* involved in the proliferation of MCF 7 cells. RNA was extracted from MCF-7 cells after the treatment with cytarabine and FCCNPs for 48 h with IC_{50} value of FCCNPs using TRI reagent (Sigma-Aldrich, USA) following the protocol given by the manufacturer. RNase free DNase 1 enzyme (New England Biolabs, USA) was added to RNA samples (0.2 µg $^{-1}$of RNA) from control and treated MCF 7 cells. Concentration and yield of RNA were measured using UV–Visible spectrophotometer (U-2800 Hitachi, Japan) by taking absorbance at 260/ 280 nm. The quality of RNA samples was checked by running 1% agarose gel stained with ethidium bromide. The agarose gel was visualised under ultraviolet light, documented using gel documentation (Bio-Rad, USA) system installed with Quantity One® software (Gel Doc XR+, Bio-Rad, USA). About 2 µg of RNA was reverse transcribed to cDNA. Quantitative real-time PCR analysis was performed in a Step OnePlus Real-Time PCR system (Applied Biosystems, USA) using Power SYBR Green PCR Master Mix (Applied Biosystems, UK) with reported primers (Table 1) [20,21] The expression of genes involved in cell proliferation was normalised using an endogenous housekeeping gene, *GAPDH* using ΔC_T method. The amplification cycle consists of denaturation at 94° C for 40 sec and annealing at 60° C for 45 sec, and relative gene expression was quantified by $2^{-\Delta\ \Delta\ CT}$ method [22].

2.13. Statistical analysis

All experiments were done at least three times, and the results were

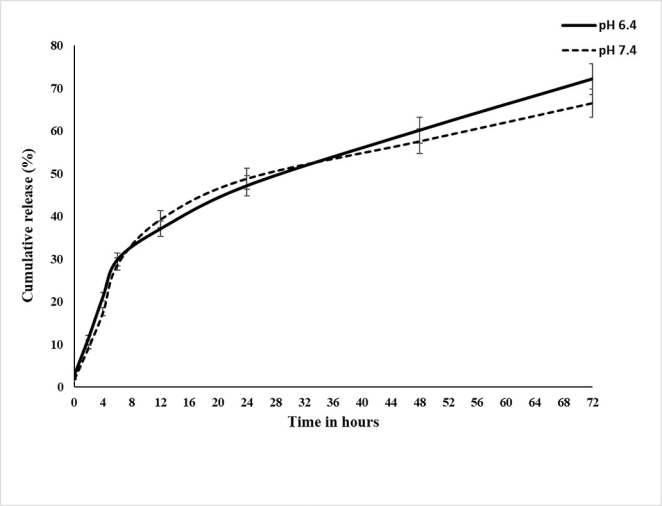

Fig. 4. The cumulative release percentage of cytarabine from folate conjugated chitosan nanoparticles at pH 6.4 and 7.4. Data were given as Mean ± SD (p value < 0.05).

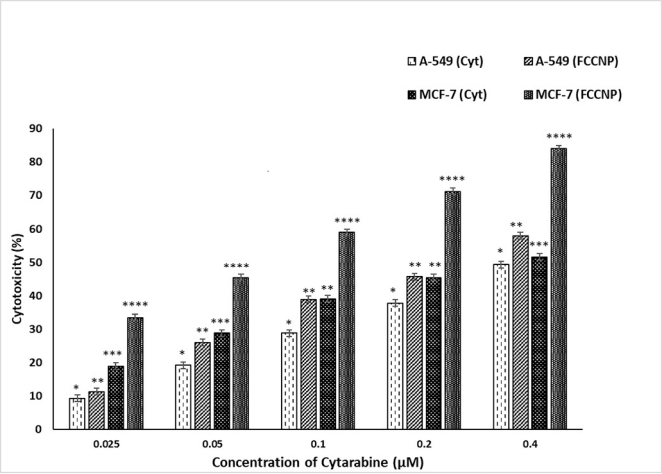

Fig. 5. MTT assay of FCCNPs in MCF-7 and A-549 cells after 72 h exposure. Results expressed as Mean ± SD (p value < 0.05).

expressed as mean ± SD. One way analysis of variance (ANOVA) followed by Tukey's post-hoc analysis using SPSS software (version 20) was used to evaluate the statistical significance, and p-value < 0.05 indicated a statistically significant difference.

3. Result and discussion

3.1. Synthesis and characterisation of folate conjugated chitosan

Folate conjugated chitosan was synthesised by aminoacylation reaction using carbodiimide. Folate was conjugated to chitosan through an amide bond in the presence of a water-soluble coupling agent, EDC and NHS. EDC activates the carboxyl group of folic acid to form an O-acylisourea intermediate which can react with an amino group of chitosan to form a stable amide bond [23]. It is reported that the γ – COOH of folic acid is more prone to conjugation due to its high reactivity [24,25]. Conjugation of folate on chitosan was characterised by FTIR and ^{1}H NMR analysis.

Fig. 1. shows the changes in the FTIR spectrum of chitosan, folic acid and folate-chitosan conjugate. The spectra of chitosan showed peaks at 1100, 1660, 2870 and 3410 cm^{-1}. The peak at 1100 of chitosan is attributed to the vibration of C-O-C bond. Folic acid showed characteristic peaks at 768, 1610, 1700, 3300 and 3540 cm^{-1} in which the peaks, 1700 and 3540 cm^{-1} corresponds to the C = O stretching and –OH stretching of carboxylic acid, respectively. Significant differences were observed in the IR spectra of FCS when compared to that of chitosan and FA. The FCS spectra showed peaks at 769, 1070, 1560, 1630 and 3430 cm^{-1}. The absorption peak of amide of chitosan at 1660 cm^{-1} was shifted to 1630 cm^{-1} in FCS spectra. The peak at 1630 cm^{-1} of FCS owes to the stretching of bonded C = O group, and the peak at 1560 corresponds to the N–H bending vibration of the secondary amide group. The conjugation was also confirmed by ^{1}H NMR (Fig. 2). The spectra of folic acid show characteristic signals at 8.65, 8.15, 7.64, 6.95, 6.66, 4.48, 4.31 and 2.32 ppm. The signals at 7.6 ppm and 6.6 ppm in the FCS spectra is attributed to the aromatic protons from folic acid, whereas the signal at 2.07 ppm corresponds to the acetamino group of chitosan. The spectra obtained from both FTIR and ^{1}H NMR revealed that the folic acid was successfully conjugated to chitosan.

3.2. Synthesis and characterisation of cytarabine loaded folate conjugated chitosan nanoparticles

Cytarabine loaded FCCNP were prepared by ionic gelation method in which the amino groups of the FCS crosslinked with the anionic group of TPP. The entrapment efficiency and drug loading capacity of the FCCNP particles was found 68.97 ± 1.24 % and 31.67 ± 0.954 % respectively. Ionic gelation is a promising strategy for encapsulating hydrophilic moieties. As a hydrophilic drug, cytarabine is easily trapped inside the polymer matrix and stabilised by electrostatic interactions and hydrogen bonds. The images obtained from TEM showed nanosized particles with an average diameter of 50 nm (Fig. 3a). DLS measurement shows a stable monodisperse nanosuspension with mean hydrodynamic diameter of 181.5 nm, polydispersity index (PDI) of 0.980 and zeta potential of FCCNPs of + 45.2 mV (Fig. 3b). The size obtained from the TEM was smaller than the size measured from DLS. The value of zeta potential of FCCNP indicates the positively charged particles that prevent aggregation and indicates a stable nano-suspension. Particles with zeta potential higher than ± 30 mV are considered as stable suspension due to the repulsive electrostatic interaction. Moreover, the high positive charge on the surface of nanoparticles facilitates the binding of particles with the negatively charged cell membrane, making it an ideal platform for drug delivery.

In vitro release of cytarabine from the FCCNPs was studied at the pH of 6.4 and 7.4 to mimic the conditions of tumour microenvironment and blood, respectively. It is reported that most human tumours exhibit pH values in the range of 6.15 – 7.4 whereas normal tissues exhibit pH in the range of 7 – 7.4 and a few tumours such as astrocytomas and squamous cell carcinomas show pH < 6 [26]. The cumulative percentage profile of cytarabine released from folate conjugated chitosan nanoparticles at regular intervals is shown in Fig. 4. A biphasic release kinetics was observed for cytarabine release i.e.; an initial burst release followed by a slow-release. It was observed that 47% of the drug was released in 24 h at pH 6.4 and 7.4 followed by a slow and sustained release. At 72 h, 72% of cytarabine was released at pH 6.4, whereas 66% was released at pH 7.4. The initial burst release of cytarabine was due to the solubilization of cytarabine adsorbed on the surface of polymer and the diffusion of drug through the polymer attributes for the slow release. The release of cytarabine was found slightly higher at the pH of tumour milieu (pH 6.4) compared to that of physiological pH (pH7.4). The pH-sensitive release enhances the accumulation of cytarabine in the tumour microenvironment compared to normal tissues of physiological pH, thereby reducing the toxic side effects of cytarabine [27]. There is an increase in the pore size of polymer matrix due to the repulsion of protonated amino groups at lower pH might be the reason for the enhanced release of the payload at pH 6.4 [28].

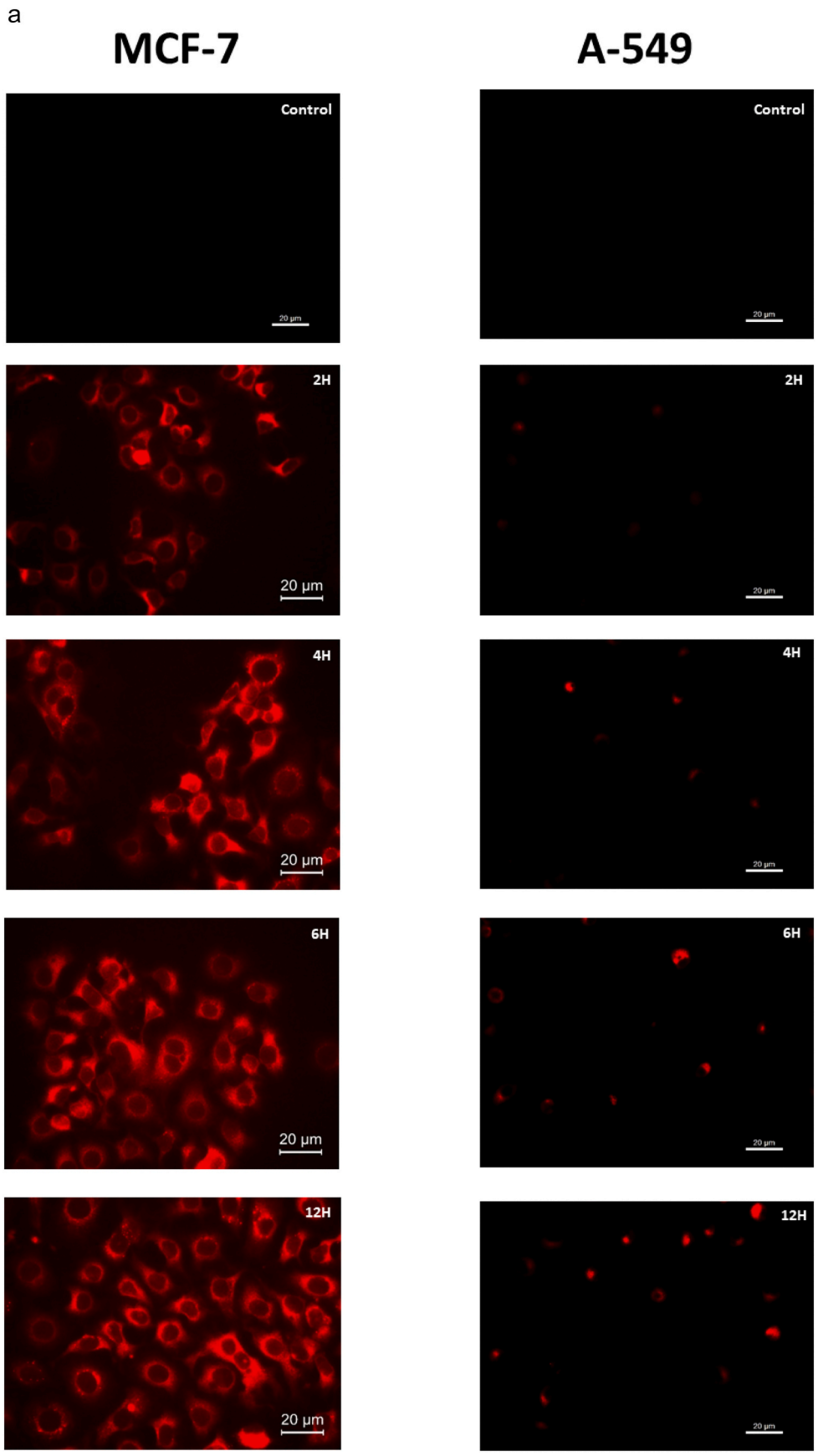

Fig. 6a. Fluorescence microscopy images of cell uptake of Squaraine 650 (SQ650) loaded FCCNPs in MCF-7 cells and A-549 cells at different time intervals (2nd, 4th, 6th and 12th hours). MCF-7 cells showing intense red fluorescence of SQ 650 while A-549 cells show very weak fluorescence.

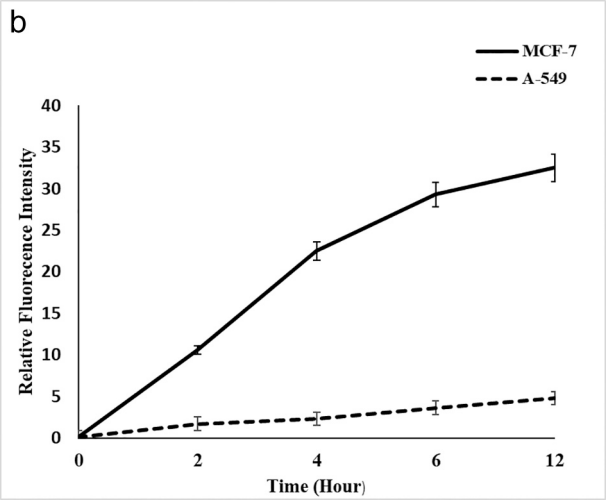

Fig. 6b. Relative fluorescence intensity measured after the incubation of SQ 650 loaded FCCNPs in MCF-7 and A-549 cells at different time intervals (2nd, 4th, 6th and 12th hours).

3.3. In vitro cytotoxicity of FCCNP

The anticancer activity of FCCNP was evaluated in MCF-7 (folate receptor positive) and A-549 (folate receptor negative) cell lines by MTT assay. In MCF-7 cells the viability was found to decrease after the treatment of FCCNP for 72 h compared with cytarabine. The IC_{50} value of FCCNP for 72 h was 0.08 ± 0.05 μM which was lower compared to that of unencapsulated cytarabine which was 0.329 ± 0.028 μM. However, cytarabine does not show cytotoxicity in A-549 cell lines in the above concentration range and the IC_{50} of FCCNP was found 0.28 ± 0.19 μM. The IC_{50} value obtained from the MTT assay showed that cytotoxicity of FCCNPs was significantly higher in MCF-7 cells when compared to A-549 cell lines (Fig. 5). It is evident from the result that the viability of the cells decreased in a dose-dependent manner. Our previous studies have shown that cytarabine loaded chitosan nanoparticles showed an increased release from chitosan nanoparticles at the pH of tumour microenvironment. The cytocompatibility of FCCNPs was also evaluated in L929 cells (non-cancerous) and found non - cytotoxic as the viability percentage is not significantly different from the control cells (Supplementary data Fig. 1). Studies have shown that folate conjugated nanoparticles in nude mice with xenograft MCF −7 tumours showed potent antitumour effects and reduced drug accumulation in non-targeted tissues [29]. The increase in cytotoxicity of FCCNP might be due to the enhancement of the internalisation of cytarabine in MCF-7 cells by receptor-mediated endocytosis and enhanced permeation and retention (EPR) effect. The endothelial cells of tumour cells have gaps around 50 to 500 nm causes the permeation and accumulation of molecules with a size<500 nm. Folate conjugation on FCCNP enhances the bioavailability of the payload through an active targeting strategy along with the EPR effect. In addition, the sustained release of the drug from nanoparticles makes continuous exposure of the drug, which contributes to an enhancement in the cytotoxic effect.

3.4. Intracellular uptake of dye loaded FCCNPs

Cell uptake of the nanoparticles in MCF-7 and A-549 cell lines were tracked using a fluorescent dye, squaraine 650. SQ 650 was loaded along with the drug cytarabine, during the synthesis of FCCNPs. SQ 650 absorbs light at the visible to IR region and show fluorescence emission properties. Due to the exhibition of fluorescence emission properties, SQ 650 was generally used for labelling. The dye loaded FCCNPs were incubated in MCF-7 and A-549 cells for 2, 4, 6 and 12 h. Control cells were taken without the treatment and images of SQ 650 loaded FCCNPs

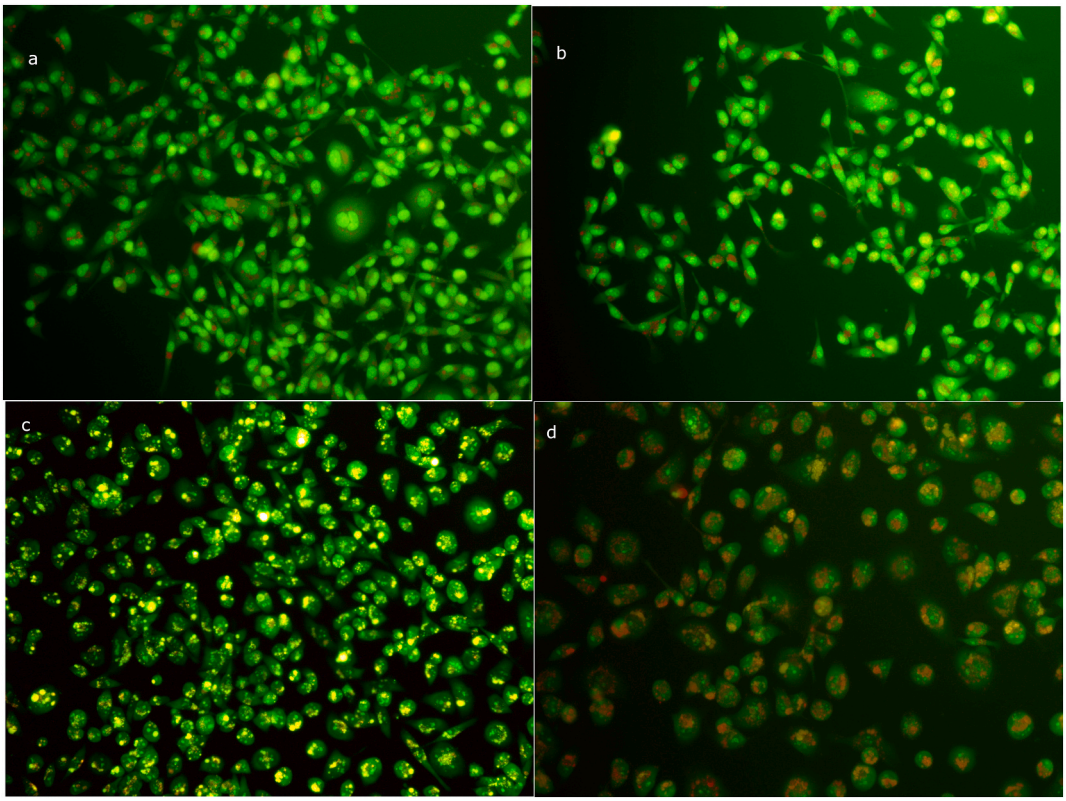

Fig. 7. Fluorescence Microscopy Images of MCF-7 cells following Acridine Orange/ Ethidium Bromide (AO/EB) staining. (a) Control (b) Blank (c) Cytarabine (d) FCCNPs.

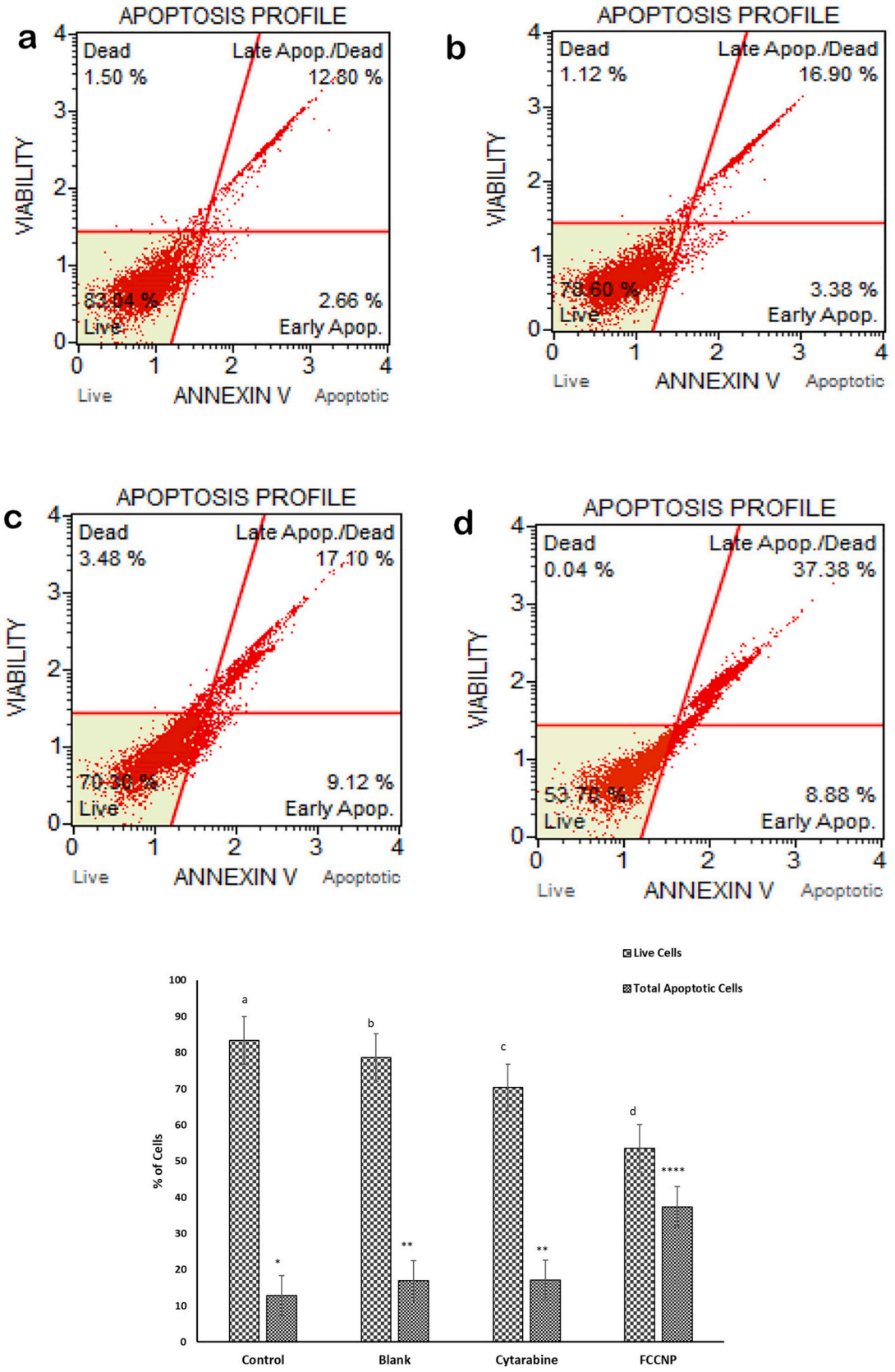

Fig. 8. Flow cytometry analysis of MCF-7 cells treated with FCCNPs. Dot plot representation of the distribution of apoptotic cells after 72 h incubation with FCCNPs followed by Annexin – PI staining. Upper right quadrant represents late apoptotic cells.
Representation of percentage of live and apoptotic cells after the treatment with cytarabine and FCCNP by flow cytometry. Data are expressed as Mean ± SD of three independent experiments SD (n – 3; p value < 0.05).

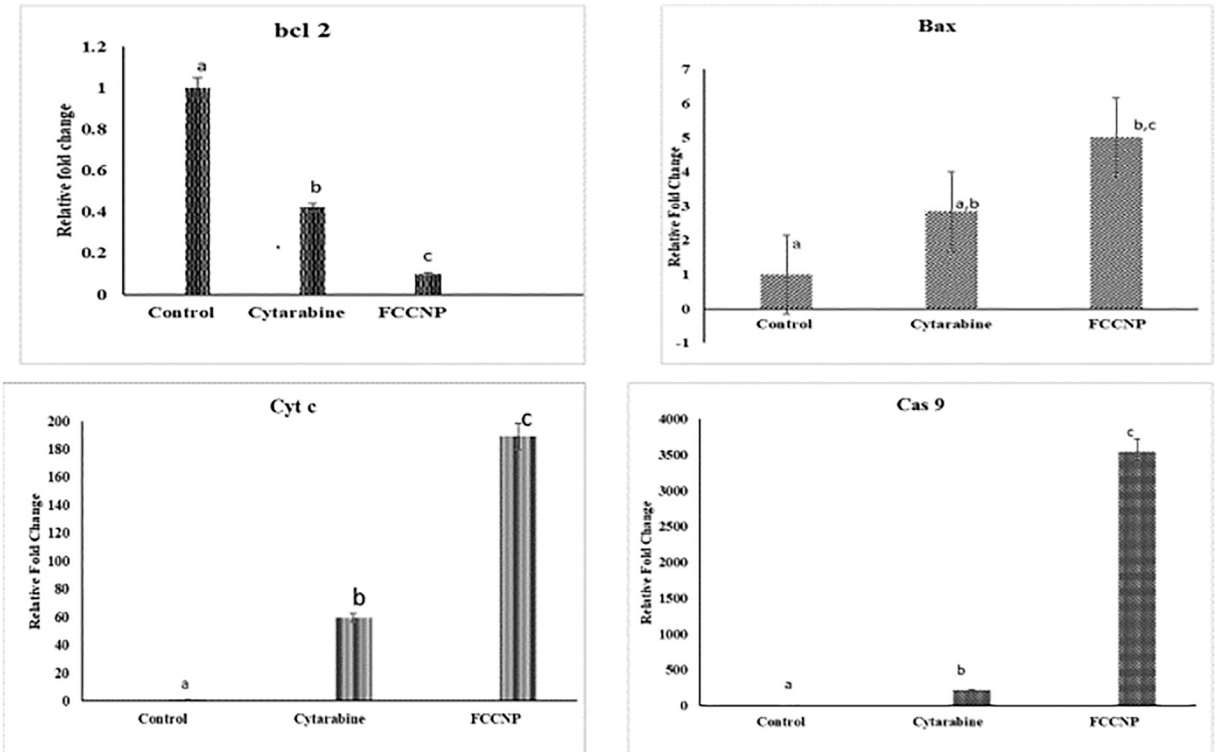

Fig. 9. Relative fold change in the expression of apoptotic genes, *bcl2, bax, cas 9* and *cytc* in MCF-7 cells after 72 h incubation with FCCNP and cytarabine. Data are expressed as Mean ± SD (n-3; p value < 0.05).

at different time intervals were recorded (Fig. 6a). In the initial four hours, red fluorescence was seen in the cytosol and around the nuclear membrane, and the nucleus showed fluorescence in the later hours. The intensity of the fluorescence in MCF-7 cells was found increasing in a linear manner and reached maximum at 6th hour and enters into a plateu afterwards whereas the relative fluorescence intensity was found very low in A-549 cells (Fig. 6b). No fluorescence was observed in the control. Cell internalisation tracking using SQ 650 validate the bioavailability of synthesised folate conjugated chitosan nanoparticles in MCF-7 cells.

3.5. Determination of apoptosis by AO/EB dual staining

Apoptosis associated morphological changes of the cell lines can be visualised using fluorescence microscopy with differential staining methods. Differential staining using intercalating dyes, acridine orange (AO), and ethidium bromide (EB) were used to evaluate cells morphological changes following FCCNP treatment. MCF-7 cells were treated with the IC_{50} concentration of cytarabine in FCCNP for 72 h and the images were recorded along with control and cells treated with blank nanoparticles (Fig. 7). Apoptosis is marked by a series of morphological changes such as cell shrinkage, rounding up with loss of contact with adjacent cells, chromatin condensation followed by fragmentation of nuclear, leading to the scattering of chromatin beads throughout the cytoplasm. Acridine orange intercalates into double-stranded DNA and emits green fluorescence [30]. Acridine orange was taken up by all cells and make live cells with bright green chromatin and organised structures. Early apoptotic cells were observed with yellowish green nuclei, and late apoptotic cells were shown by orange ethidium bromide (EB) staining. Ethidium bromide is taken up by only apoptotic cells as they lost the cell membrane integrity. Late apoptotic cells displayed orange coloured condensed and fragmented chromatin. The control cells without any treatment showed bright green nuclei, indicative of viable cells. However, the cells treated with FCCNP showed asymmetrically located orange ethidium bromide staining.

3.6. Annexin V assay

Annexin V assay was used to quantify extent of apoptosis after FCCNP treatment for 72 h using a flow cytometer. Annexin V-FITC, along with propidium iodide differentiates the live and apoptotic cells [31]. Apoptosis was characterised by the disruption of the integrity of cell membrane, which can be detected by Annexin V assay. One of the changes of early apoptosis is the translocation of phosphatidyl serine on the outer surface of plasma membrane [32]. However, the cell membrane remains intact during the early phases of apoptotic cell death. FITC labelled Annexin V binds to the phosphatidyl serine due to the phospholipid binding affinity of Annexin V protein and shows green fluorescence indicative of early apoptosis detected by flow cytometer [33]. Propidium iodide (PI) was used to identify late apoptosis and necrotic cells as it enters these cells due to the loss of plasma membrane integrity. Cells having damaged cell membrane shows red fluorescence induced by PI while the early apoptotic cells exclude PI. Cells were treated with IC_{50} of FCCNP (0.08 μM) and compared with cells treated with cytarabine alone and blank nanoparticles. Fig. 8a showed the population profile of live and apoptotic cells stained with Annexin V and PI. It was found that the apoptotic cells incubated with cytarabine alone were 20.31 ± 0.03 % whereas the percentage of apoptotic cells was increased to 46.32 ± 0.07 % when treated with FCCNP (Fig. 8b). FACS results showed that there was an increased percentage of apoptotic cells when cytarabine was incorporated into nanoparticles.

3.7. qRT -PCR analysis for relative expression of apoptotic genes

The expression of genes involved in the proliferation of MCF-7 cells was quantified, and the relative fold change in the expression after the treatment of cytarabine and FCCNPs was determined by qRT-PCR. The expression levels of genes in MCF −7 cells without drug treatment were taken as a control for normalising expression levels in treatment groups, and the relative expression was calculated by $2^{-\Delta\Delta CT}$ method. Cells treated with cytarabine and FCCNPs showed downregulation of *bcl2*

gene expression, whereas the expression of genes, *bax, cyt c* and *cas 9* significantly increased after 72 h (Fig. 9). Precisely FCCNP treated cells showed 1.76-fold increase in *bax* expression, 3.18-fold increase in *cyt c* and 16.5-fold increase in *cas 9* with respect to that of cytarabine treated cells. It has been reported that *bcl2* is overexpressed in carcinomas and inhibits apoptosis, whereas *bax* overexpression induces apoptosis [33]. In this study, *bcl2* expression was downregulated 4-fold when compared to cytarabine which might lead to the activation of apoptosis in FCCNP treated cells. The *bax / bcl 2* ratio of FCCNP showed 12-fold increase in FCCNP treated cells when compared to cytarabine treated MCF-7 cells. The obtained ratio indicates the enhanced susceptibility of cells to apoptosis. The increased expression of pro-apoptotic gene, *bax* and the decreased expression of anti-apoptotic gene, *bcl 2* in FCCNP treated cells is a clear indication of increased anticancer effect by folate conjugated chitosan nanoparticles with cytarabine. Previous studies reported an inverse relationship between *bcl 2* expression and regulation of apoptosis in MCF 7 cells after treatment with silver nanoparticles [34]. Over the above the increased expression of *cyt c* plays a key role in apoptosis such as morphological changes of nucleus, DNA fragmentation and translocation of phosphatidyl serine on the cell surface [35]. Treatment with FCCNPs showed overexpression of *bax, cyt c* and *cas9*, which indicates the induction of mitochondrial dependent intrinsic pathway of apoptosis in MCF 7 cells.

4. Conclusion

In this study, cytarabine was loaded to folate modified chitosan nanoparticles to evaluate the enhanced efficiency of cytotoxicity in FR positive MCF-7 cell lines. Cytarabine loaded folate conjugated chitosan nanoparticles were synthesised by ionic gelation method. The obtained FCCNPs showed desirable size and positive surface charge for targeting cancer cells. Cytotoxicity studies showed a significant decrease in cell viability by FCCNP treatment than free cytarabine, which was supported by the apoptotic studies by AO/EB dual staining and Annexin V flow cytometry. Increased expression of *bax, cyt c* and *cas 9* indicates the activation of the intrinsic pathway of apoptosis in FCCNP treated MCF-7 cells. The present in vitro study confirms that folate conjugated chitosan nanoparticles improved the cytotoxicity of cytarabine in human breast adenocarcinoma cell lines (MCF-7). However, an in vivo evaluation of FCCNP in a suitable animal model is essential to establish its improved anticancer effects.

CRediT authorship contribution statement

Deepa Geethakumari: Conceptualization, Methodology, Formal analysis, Data curation, Investigation, Writing – original draft. **Anoop Bhaskaran Sathyabhama:** Methodology, Formal analysis, Data curation. **Krishnapriya Raji Sathyan:** Methodology, Formal analysis, Investigation, Data curation. **Dhaneesha Mohandas:** Methodology, Formal analysis, Investigation. **Jisha V. Somasekharan:** Methodology, Writing – review & editing. **Sajeevan Thavarool Puthiyedathu:** Conceptualization, Methodology, Writing – review & editing, Supervision, Project administration.

Declaration of Competing Interest

The authors declare that they have no known competing financial interests or personal relationships that could have appeared to influence the work reported in this paper.

Acknowledgement

The first author is thankful to University Grants Commission (UGC), India, Government of India for the BSR fellowship. The authors acknowledge the Sophisticated Test and Instrumentation Centre (STIC) and National Centre for Aquatic Animal Health (NCAAH), Cochin University of Science and Technology for the facilities provided.

Appendix A. Supplementary data

Supplementary data to this article can be found online at https://doi.org/10.1016/j.ijbiomac.2021.12.070.

References

[1] J. Liu, D. Zhao, W. He, H. Zhang, Z. Li, Y. Luan, Nanoassemblies from amphiphilic cytarabine prodrug for leukemia targeted therapy, J. Colloid Interface Sci. 487 (2017) 239–249, https://doi.org/10.1016/j.jcis.2016.10.041.
[2] P. Vega-Vásquez, N.S. Mosier, J. Irudayaraj, Nanoscale Drug Delivery Systems: From Medicine to Agriculture, Front. Bioeng, Biotechnol. 8 (2020) 1–16, https://doi.org/10.3389/fbioe.2020.00079.
[3] S. Parveen, S.K. Sahoo, Evaluation of cytotoxicity and mechanism of apoptosis of doxorubicin using folate-decorated chitosan nanoparticles for targeted delivery to retinoblastoma, Cancer Nanotechnol. 1 (1-6) (2010) 47–62, https://doi.org/10.1007/s12645-010-0006-0.
[4] G. Deepa, N. Ashwanikumar, J.J. Pillai, G.S.V. Kumar, Polymer Nanoparticles - A Novel Strategy for Administration of Paclitaxel in Cancer Chemotherapy, Curr. Med. Chem. 19 (2012) 6207–6213, https://doi.org/10.2174/092986731120906620 7.
[5] M. Prabaharan, Chitosan-based nanoparticles for tumor-targeted drug delivery, Int. J. Biol. Macromol. 72 (2015) 1313–1322, https://doi.org/10.1016/j.ijbiomac.2014.10.052.
[6] Y.H. Bae, K. Park, Targeted drug delivery to tumors: Myths, reality and possibility, J. Control. Release. 153 (3) (2011) 198–205, https://doi.org/10.1016/j.jconrel.2011.06.001.
[7] L. Keawchaoon, R. Yoksan, Preparation, characterization and in vitro release study of carvacrol-loaded chitosan nanoparticles, Colloids Surfaces B Biointerfaces. 84 (1) (2011) 163–171, https://doi.org/10.1016/j.colsurfb.2010.12.031.
[8] J.F. Ross, P.K. Chaudhuri, M. Ratnam, Differential regulation of folate receptor isoforms in normal and malignant tissues in vivo and in established cell lines. Physiologic and clinical implications, Cancer. (1994), https://doi.org/10.1002/1097-0142(19940501)73:9<2432::AID-CNCR2820730929>3.0.CO;2-S.
[9] B. Bahrami, M. Mohammadnia-Afrouzi, P. Bakhshaei, Y. Yazdani, G. Ghalamfarsa, M. Yousefi, S. Sadreddini, F. Jadidi-Niaragh, M. Hojjat-Farsangi, Folate-conjugated nanoparticles as a potent therapeutic approach in targeted cancer therapy, Folate-conjugated nanoparticles as a potent therapeutic approach in targeted cancer therapy 36 (8) (2015) 5727–5742, https://doi.org/10.1007/s13277-015-3706-6.
[10] Y. Zu, Q. Zhao, X. Zhao, S. Zu, L. Meng, Process optimization for the preparation of nanoparticles as a tumor-targeted drug delivery system using a two-level factorial design method (2011) 3429–3441.
[11] L. Xu, Q. Bai, X. Zhang, H. Yang, Folate-mediated chemotherapy and diagnostics: an updated review and outlook, J. Control. Release. 28 (2018) 73–82, https://doi.org/10.1016/j.jconrel.2017.02.023.Folate-mediated.
[12] A. Yassemi, S. Kashanian, H. Zhaleh, Folic acid receptor-targeted solid lipid nanoparticles to enhance cytotoxicity of letrozole through induction of caspase-3 dependent-apoptosis for breast cancer treatment, Pharm. Dev. Technol. 25 (4) (2020) 397–407, https://doi.org/10.1080/10837450.2019.1703739.
[13] A. Amer Ridha, S. Kashanian, R. Rafipour, A. Hemati Azandaryani, H. Zhaleh, E. Mahdavian, A promising dual-drug targeted delivery system in cancer therapy: nanocomplexes of folate–apoferritin-conjugated cationic solid lipid nanoparticles, Pharm. Dev. Technol. 26 (6) (2021) 673–681, https://doi.org/10.1080/10837450.2021.1920037.
[14] L. Cheng, H. Ma, M. Shao, Q. Fan, H. Lv, J. Peng, T. Hao, D. Li, C. Zhao, X. Zong, Synthesis of folate-chitosan nanoparticles loaded with ligustrazine to target folate receptor positive cancer cells, Mol Med Rep. 16 (2) (2017) 1101–1108, https://doi.org/10.3892/mmr.2017.6740.
[15] K.K. Yang, M. Kong, Y.N. Wei, Y.a. Liu, X.J. Cheng, J. Li, H.J. Park, X.G. Chen, Folate-modified-chitosan-coated liposomes for tumor-targeted drug delivery, J. Mater. Sci. 48 (4) (2013) 1717–1728, https://doi.org/10.1007/s10853-012-6930-0.
[16] P. Calvo, C. RemunanLopez, J.L. VilaJato, M.J. Alonso, C. Remuñan-López, J. L. Vila-Jato, M.J. Alonso, Chitosan and chitosan ethylene oxide propylene oxide block copolymer nanoparticles as novel carriers for proteins and vaccines, Pharm. Res. 14 (1997) 1431–1436, https://doi.org/10.1023/A:1012128907225.
[17] M. Dhaneesha, O. Hasin, K.C. Sivakumar, R. Ravinesh, C.B. Naman, S. Carmeli, T. P. Sajeevan, DNA Binding and Molecular Dynamic Studies of Polycyclic Tetramate Macrolactams (PTM) with Potential Anticancer Activity Isolated from a Sponge-Associated Streptomyces zhaozhouensis subsp. mycale subsp. nov, Mar. Biotechnol. 21 (1) (2019) 124–137, https://doi.org/10.1007/s10126-018-9866-9.
[18] L. Li, D. Patil, G. Petruncio, K.K. Harnden, J.V. Somasekharan, M. Paige, L. V. Wang, C. Salvador-Morales, Integration of Multitargeted Polymer-Based Contrast Agents with Photoacoustic Computed Tomography: An Imaging Technique to Visualize Breast Cancer Intratumor Heterogeneity, ACS Nano. 15 (2) (2021) 2413–2427, https://doi.org/10.1021/acsnano.0c0589310.1021/acsnano.0c05893.s001.
[19] D. Ribble, N.B. Goldstein, D.A. Norris, Y.G. Shellman, A simple technique for quantifying apoptosis in 96-well plates, BMC Biotechnol. 5 (2005) 1–7, https://doi.org/10.1186/1472-6750-5-12.

[20] Y. Asara, J.A. Marchal, E. Carrasco, H. Boulaiz, G. Solinas, P. Bandiera, M. A. Garcia, C. Farace, A. Montella, R. Madeddu, Cadmium modifies the cell cycle and apoptotic profiles of human breast cancer cells treated with 5-fluorouracil, Int. J. Mol. Sci. 14 (2013) 16600–16616, https://doi.org/10.3390/ijms140816600.
[21] D.N. Zacks, Q.D. Zheng, Y. Han, R. Bakhru, J.W. Miller, FAS-mediated apoptosis and its relation to intrinsic pathway activation in an experimental model of retinal detachment, Investig. Ophthalmol. Vis. Sci. 45 (2004) 4563–4569, https://doi.org/10.1167/iovs.04-0598.
[22] K.J. Livak, T.D. Schmittgen, Analysis of relative gene expression data using real-time quantitative PCR and the 2-ΔΔCT method, Methods. 25 (4) (2001) 402–408, https://doi.org/10.1006/meth.2001.1262.
[23] D. Vllasaliu, L. Casettari, G. Bonacucina, M. Cespi, G. Palmieri, L. Illum, Folic Acid Conjugated Chitosan Nanoparticles for Tumor Targeting of Therapeutic and Imaging Agents, Pharm. Nanotechnol. 1 (2013) 184–203, https://doi.org/10.2174/22117385113019990001.
[24] Z. Zhang, S. Huey Lee, S.-S. Feng, Folate-decorated poly(lactide-co-glycolide)-vitamin E TPGS nanoparticles for targeted drug delivery, Biomaterials. 28 (10) (2007) 1889–1899, https://doi.org/10.1016/j.biomaterials.2006.12.018.
[25] J. Ji, D. Wu, L.i. Liu, J. Chen, Y.i. Xu, Preparation, characterization, and in vitro release of folic acid-conjugated chitosan nanoparticles loaded with methotrexate for targeted delivery, Polym. Bull. 68 (6) (2012) 1707–1720, https://doi.org/10.1007/s00289-011-0674-x.
[26] P. Vaupel, F. Kallinowski, P. Okunieff, Blood Flow, Oxygen and Nutrient Supply, and Metabolic Microenvironment of Human Tumors: A Review, Cancer Res. 49 (1989) 6449–6465.
[27] G. Deepa, K.C. Sivakumar, T.P. Sajeevan, Molecular simulation and in vitro evaluation of chitosan nanoparticles as drug delivery systems for the controlled release of anticancer drug cytarabine against solid tumours, 3, Biotech. 8 (2018) 1–11, https://doi.org/10.1007/s13205-018-1510-x.
[28] H. Zhang, S. Mardyani, W.C.W. Chan, E. Kumacheva, Design of biocompatible chitosan microgels for targeted pH-mediated intracellular release of cancer therapeutics, Biomacromolecules. 7 (5) (2006) 1568–1572, https://doi.org/10.1021/bm050912z.
[29] A. Martínez, E. Muñiz, C. Teijón, I. Iglesias, J.M. Teijón, M.D. Blanco, Targeting tamoxifen to breast cancer xenograft tumours: Preclinical efficacy of folate-attached nanoparticles based on alginate-cysteine/disulphide- bond-reduced albumin, Pharm. Res. 31 (5) (2014) 1264–1274, https://doi.org/10.1007/s11095-013-1247-5.
[30] C. Renvoizé, A. Biola, M. Pallardy, J. Bréard, Apoptosis: Identification of dying cells, Cell Biol. Toxicol. 14 (1998) 111–120, https://doi.org/10.1023/A:1007429904664.
[31] M. Dhaneesha, M.d. Umar, T.S. Merlin, K.P. Krishnan, V. Sukumaran, R.K. Sinha, A. Anas, P. Fu, J.B. MacMillan, T.P. Sajeevan, Pseudonocardia cytotoxica sp. nov., a novel actinomycete isolated from an Arctic fjord with potential to produce cytotoxic compound, Antonie van Leeuwenhoek, Int. J. Gen Mol. Microbiol. 114 (1) (2021) 23–35, https://doi.org/10.1007/s10482-020-01490-7.
[32] I. Vermes, C. Haanen, H. Steffens-Nakken, C. Reutellingsperger, A novel assay for apoptosis Flow cytometric detection of phosphatidylserine expression on early apoptotic cells using fluorescein labelled Annexin V, J. Immunol. Methods. 184 (1) (1995) 39–51, https://doi.org/10.1016/0022-1759(95)00072-I.
[33] A. Boroumand Moghaddam, M. Moniri, S. Azizi, R. Abdul Rahim, A. Bin Ariff, M. Navaderi, R. Mohamad, Eco-friendly formulated zinc oxide nanoparticles: Induction of cell cycle arrest and apoptosis in the MCF-7 cancer cell line, Genes (Basel) 8 (10) (2017) 281, https://doi.org/10.3390/genes8100281.
[34] J. Baharara, F. Namvar, T. Ramezani, M. Mousavi, R. Mohamad, Silver nanoparticles biosynthesized using Achillea biebersteinii flower extract: Apoptosis induction in MCF-7 cells via caspase activation and regulation of bax and bcl-2 gene expression, Molecules. 20 (2015) 2693–2706, https://doi.org/10.3390/molecules20022693.
[35] N. Kanipandian, D. Li, S. Kannan, Induction of intrinsic apoptotic signaling pathway in A549 lung cancer cells using silver nanoparticles from Gossypium hirsutum and evaluation of in vivo toxicity, Biotechnol. Reports. 23 (2019) e00339, https://doi.org/10.1016/j.btre.2019.e00339.